SIMULATION OF SEMICONDUCTOR DEVICES AND PROCESSES Vol. 4
Edited by W. Fichtner, D. Aemmer - Zurich (Switzerland) September 12-14, 1991 - Hartung-Gorre

One-dimensional Simulation of a Bipolar Transistor by means of Spherical Harmonics Expansion of the Boltzmann Transport Equation *

Antonio Gnudi, Davide Ventura, and Giorgio Baccarani

Dipartimento di Elettronica, Informatica e Sistemistica
Università di Bologna, viale Risorgimento 2
40136 Bologna, Italy

Abstract

A one-dimensional n-p-n BJT has been simulated by expanding the Boltzmann Transport Equation (BTE) in spherical harmonics. The solution provides the energy distribution of electrons as a function of position in the entire device with a reasonable CPU time. We compare the average velocity and energy with results of the hydrodynamic model.

1 Introduction

Modeling hot electron effects in silicon is a challenging task which has gained increasing popularity in recent years. The aim is typically that of predicting substrate current and hot-carrier injection into the gate oxide in MOSFET's, or impact ionization within the collector space-charge region of BJT's. The most common approaches in the literature are: *i)* the *hydrodynamic* (HD) model, and *ii)* the *Monte Carlo* (MC) particle simulation. The former can provide the first moments of the distribution function, such as mean velocity and energy, with good accuracy and little computational effort, but does not give any information on the high-energy tail. The latter, instead, can easily account for detailed physical effects at the expense of very large computational resources. Some proposals have been made to overcome the above limitations [1-4]. The basic idea in these papers is that of deriving from the BTE a simpler equation in the energy space by expanding the distribution function into a suitable set of basis functions. With some further simplifying assumptions, such as high energy and constant effective mass, an approximate analytical solution to the resulting equations can be worked out [2]. Otherwise, the problem can be tackled numerically. In [3] a numerical solution for the homogeneous conditions and constant electric field was obtained, and ionization coefficients were calculated in good agreement with experimental values. In [4], the expansion is extended up to the second spherical harmonics, and the band structure is generalized according to [5].

In this work we use a spherical harmonics expansion to reduce the BTE to the energy-space domain (E, x). We show how the resulting system of equations can be solved numerically in one-dimension and apply this technique to obtain the electron energy distribution pointwise in a one-dimensional *n-p-n* BJT; next we compare the average velocity and energy with results from HD calculations. While the first moments can be approximately obtained with the HD model, the high-energy part of the distribution is not simply related to any average quantity.

*Work supported by IBM, Essex Junction VT, 05452 - USA

2 Mathematical model

We begin with expanding the distribution function f in series of spherical harmonics:

$$f(\mathbf{r},\mathbf{k}) = f_0(\mathbf{r},k) + f_1(\mathbf{r},k)\cos\theta + f_2(\mathbf{r},k)\frac{1}{2}(3\cos^2\theta - 1) + ... \tag{1}$$

where θ is the angle between the crystal momentum $\mathbf{k}$ and the current density $\mathbf{J}$. A system of equations for the unknown functions f_i is obtained by substituting the expression (1) into the BTE and equating the coefficients of the harmonics of the same order. The procedure is quite general. Considering acoustic and optical phonon interactions, as well as ionized impurity scattering, and a spherically symmetric band structure, the equations for f_0 and f_1 in the (E,x) domain, in one-dimension, are

$$\frac{\partial}{\partial x}f_1 - qF\left(\frac{\partial}{\partial E}f_1 + \frac{1}{\gamma}\frac{\mathrm{d}\gamma}{\mathrm{d}E}f_1\right) = \tag{2,a}$$

$$\frac{3c_{op}}{u_g}\left\{g(E+\hbar\omega_{op})\left[N^+ f_0(E+\hbar\omega_{op}) - N f_0(E)\right] - g(E-\hbar\omega_{op})\left[N^+ f_0(E) - N f_0(E-\hbar\omega_{op})\right]\right\}$$

$$\frac{\partial}{\partial x}f_0 - qF\frac{\partial}{\partial E}f_0 + \frac{1}{\lambda}f_1 = 0 \tag{2,b}$$

In the above equations, $\gamma(E)$ is the band-shape function, $g(E)$ the density of states, u_g is the group velocity, N the optical phonon occupation number, $N^+ = N+1$, $\hbar\omega_{op}$ and c_{op} the optical phonon energy and scattering probability, respectively, F the electric field and, finally, $\lambda(E)$ the carrier mean free path which, for the aforementioned scattering mechanisms, is expressed as

$$\lambda(E) = \frac{u_g(E)}{c_{ac}\,g(E) + c_{op}\,N^+\,g(E-\hbar\omega_{op}) + c_{op}\,N\,g(E+\hbar\omega_{op}) + c_{imp}(E,N_i)g(E)} \tag{3}$$

In (3) c_{ac} is the acoustic-phonon and c_{imp} the effective ionized-impurity scattering probability. The latter depends on energy E and impurity concentration N_i.

The phonon coupling constants and the band structure are taken from [5]. More precisely, we have so far taken into account the two lowest bands of the model given in [5], thus fitting the density of states up to 2.6 eV, much beyond the parabolic band approximation. Ionized impurity scattering is treated in the Brooks-Herring formulation. The screening length is adjusted so as to match the empirical mobility model [6].

Eqs. (2) can be expressed in a more compact form using the transformation of variables $H \equiv E - q\phi(x)$, where $\phi(x)$ is the electric potential and H the total energy. By defining the coefficients of the expansion in the new space

$$f_i(E,x) = f_i(H + q\phi(x), x) \equiv \mathcal{F}_i(H,x) \tag{4}$$

equations (2) become

$$\frac{\partial}{\partial x}\left[g\lambda u_g\frac{\partial \mathcal{F}_0}{\partial x}\right] + 3c_{op}\,g(H)\big(g(H+\hbar\omega_{op})\left[N^+\mathcal{F}_0(H+\hbar\omega_{op}) - N\mathcal{F}_0(H)\right] -$$

$$-g(H-\hbar\omega_{op})\left[N^+\mathcal{F}_0(H) - N\mathcal{F}_0(H-\hbar\omega_{op})\right]\big) = 0 \tag{5,a}$$

$$\mathcal{F}_1 = -\lambda\frac{\partial \mathcal{F}_0}{\partial x} \tag{5,b}$$

where the relation $g = (8\pi m^*\gamma)/(\hbar^3 u_g)$ has been applied. Eq. (5,a) is the continuity equation in the (E,x) space, which approximates the original BTE in the $(\mathbf{k},x)$ space.

3 Numerical method

Eq. (5,a) is a second order linear difference-differential equation with non-constant coefficients, defined in the two-dimensional domain (H, x) with curvilinear boundaries $x = 0$, $x = l_{max}$, and $-q\phi(x) \leq H \leq E_{max} - q\phi(x)$, where E_{max} is the energy at the top of the second band. Equilibrium distributions are assumed at the boundaries $x = 0$ and $x = l_{max}$. The discretization grid is composed by nodes at constant total energy H, uniformly spaced in energy by intervals $\Delta H = \hbar\omega_{op}/n$, with n integer. A remarkable feature of (5,a) is the absence of partial derivatives with respect to H. Therefore, each node of coordinates (H, x) is connected along the H direction only with the nodes at $(H + \hbar\omega_{op}, x)$ and $(H - \hbar\omega_{op}, x)$, via the difference operator. The resulting algebraic system is thus composed by n decoupled subsystems, which can be solved independently with a considerable speed-up of the computation.

4 Results

The simulated structure is a one-dimensional n-p-n BJT similar to the one investigated in [7]. Piecewise uniform impurity concentration has been assumed within the emitter, base, collector and subcollector regions (Fig. 1). Two cases have been considered, namely, n and p collector regions, which are known to provide qualitatively different electric field shapes. Simulations performed with the hydrodynamic version of the code HFIELDS, with a base-emitter voltage $V_{BE} = 0.97\,\mathrm{V}$ and a collector-base voltage $V_{CB} = 3\,\mathrm{V}$, provided the electric-field profiles of Fig. 2. The base-emitter voltage has been selected such that the electron current density turns out to be about $10^5\,\mathrm{A/cm^2}$. As bandgap narrowing due to heavy doping is neglected in this study, the value of V_{BE} is somewhat overestimated. As expected, in the n^+-p-n^--n^+ case the peak electric field is located at the base-collector junction while, in the n^+-p-p^--n^+ case, the field peaks at the subcollector junction [7].

Figs. 3 and 4 compare the electron velocity and normalized energy profiles resulting from the HD program and from the solution of the present model. In the HD model mobility parameters, saturation velocity, and the energy relaxation time have been calculated by means of a best fitting procedure of the average velocity and the mean energy vs. field curves obtained with the present approximate solution of the BTE in homogeneous conditions. As far as the energy is concerned (Fig. 4), the agreement is fairly good, even if the HD model tends to provide slightly lower energies in the rising part of the curve. Also, the peak velocities at the base-collector junction are in excellent agreement (Fig. 3). On the contrary, the HD model tends to overestimate the electron velocity at the subcollector edge of the space charge region, characterized by very large negative gradients of the energy. It has been already pointed out in [8] how the HD model can hardly control the velocity in such regions.

The electron velocity profiles are illustrated in Fig. 5. Due to the larger value of the electric field at the base-collector junction, the electron peak velocity is larger in the n-collector transistor. In the depletion region, however, the situation reverses due to the different behavior of the electric-field profiles.

In Fig. 6 the electron energy profiles resulting from the simplified solution of the BTE are compared for the two BJT structures. The p-collector transistor exhibits a higher energy peak: this is due to the increasing electric field as electrons move toward the subcollector. On the other hand, in the n-collector transistor the peak field occurs at the base-collector junction, where electrons are still cold. As the electron energy increases, the electric field decreases, thus leading to a relatively flat energy over most of the collector space-charge region.

Fig. 7 shows the electron distribution in the (E, x) space for the n^+-p-p^--n^+ device. In the picture, the numerical solution obtained on the discretization grid has been interpolated on a regular and coarser grid. One can clearly see the heating of the tail of the distribution as electrons move deeper and deeper into the collector, while quasi-equilibrium distributions are observed in the emitter and in the base regions. Two populations seem to coexist within the subcollector, as revealed by two different slopes of the distribution for high and low energies: hot electrons travelling across the collector space-charge region, and majority carriers in quasi-equilibrium conditions. The energy of the tail decays slowly toward the contact, where the equilibrium boundary condition is forced. This is likely to be an unphysical effect due to the absence in our model of electron-electron interaction, which is known to push the distribution toward local equilibrium.

Two different sections of the distribution of the previous picture are shown in Fig. 8 (the normalization is such that $\int f g \, dE = 1$), at two points in the space charge region where the average energies are very nearly the same. Section $x = 0.15\,\mu$m is located in the rising part of the electron energy, whereas section $x = 0.2\,\mu$m is located at the subcollector junction, where the average energy is rapidly decreasing. As can be seen, the high-energy tail behaves very differently in the two cases. Hence, any impact-ionization model purely based on electron temperature could provide unreliable results.

5 Conclusions

In this work we have applied the spherical harmonics expansion technique to the BTE for obtaining the distribution of electrons in the (E, x) space in a one-dimensional bipolar transistor. Our model accounts for acoustic and optical phonon scattering as well as non-parabolicity effects. The average velocity and energy profiles are in good agreement with the results of the hydrodynamic model, while the high-energy shape of the distribution clearly shows the limitations of any hot-electron model based directly on the mean energy. We realize that a realistic description of the physics of high-energy electrons should also include the two upper bands of the model in [5], as well as impact ionization and electron-electron scattering. Besides, in order to fully assess the validity of approximating the distribution function with the two lower order harmonics, detailed comparisons with MC simulations are required. This will be the object of our future work. So far, we can conclude that the method presents very attractive features, considered the amount of information obtainable with a computational burden many times smaller than any MC simulation.

Acknowledgements

The authors gratefully acknowledge many helpful discussions with Drs. D. Cole and F. Odeh.

References

1. N. Goldsman, J. Frey, "Electron energy distribution for calculation of gate leakage current in MOSFET's", *Solid-State Electronics,* vol. 31, no. 6, 1988, pp. 1089–1092.

2. W. Haensch, A. v. Schwerin, "A new approach to calculate the substrate current and oxide injection in a metal-oxide-semiconductor field-effect transistor", *J. Appl. Phys.,* vol. 66, no. 3, 1989, pp. 1435–1438.

3. N. Goldsman, Y. Wu, J. Frey, "Efficient calculation of ionization coefficients in silicon

from the energy distribution function", *J. Appl. Phys.*, vol. 68, no. 3, 1990, pp. 1075–1081

4. D. Ventura, A. Gnudi, G. Baccarani, "An efficient method for evaluating the energy distribution of electrons in semiconductors based on the spherical harmonics expansion", to be presented at *1991 International Workshop on VLSI Process and Device Modeling*, Oiso, Japan, May 27-29, 1991

5. R. Brunetti, C. Jacoboni, F. Venturi, E. Sangiorgi, B. Riccò, "A many-band silicon model for hot-electron transport at high energies", *Solid-State Electronics*, vol. 32, no. 12, 1989, pp. 1663–1667

6. D. M. Caughey, R. E. Thomas, "Carrier mobilities in silicon empirically related to doping and field", *Proc. IEEE*, vol. 52, 1967, pp. 2192–2193

7. E. F. Crabbé, J. M. C. Stork, G. Baccarani, M. V. Fischetti, S. E. Laux, "The impact of non-equilibrium transport on breakdown and transit time in bipolar transistors", *IEDM-90 Tech. Dig.*, pp. 463–466, 1990

8. A. Gnudi, F. Odeh, M. Rudan, "Investigation of non-local transport phenomena in small semiconductor devices", *European Trans. on Tel.*, vol. 1, pp. 307–312, 1990

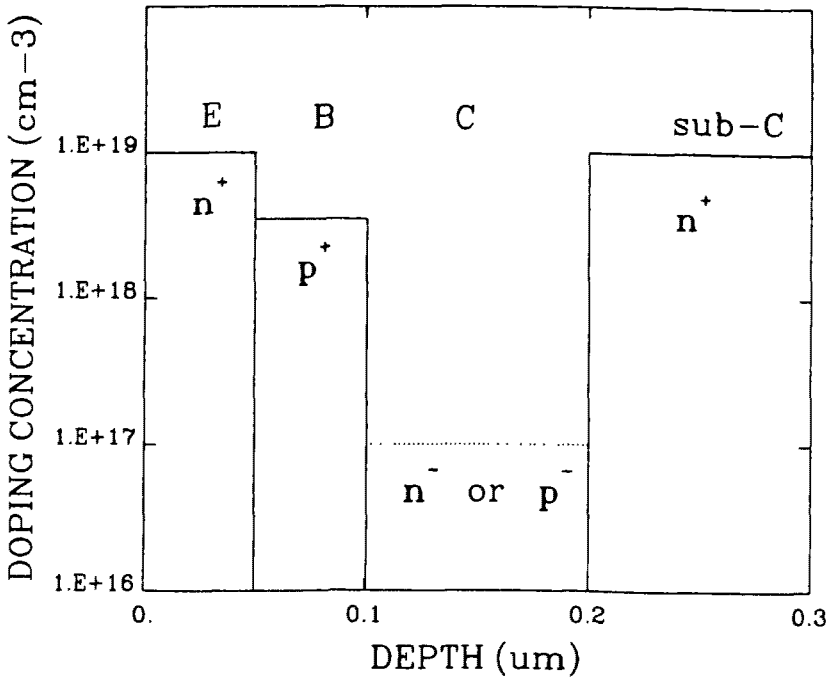

Fig. 1. Doping profiles of the simulated devices.

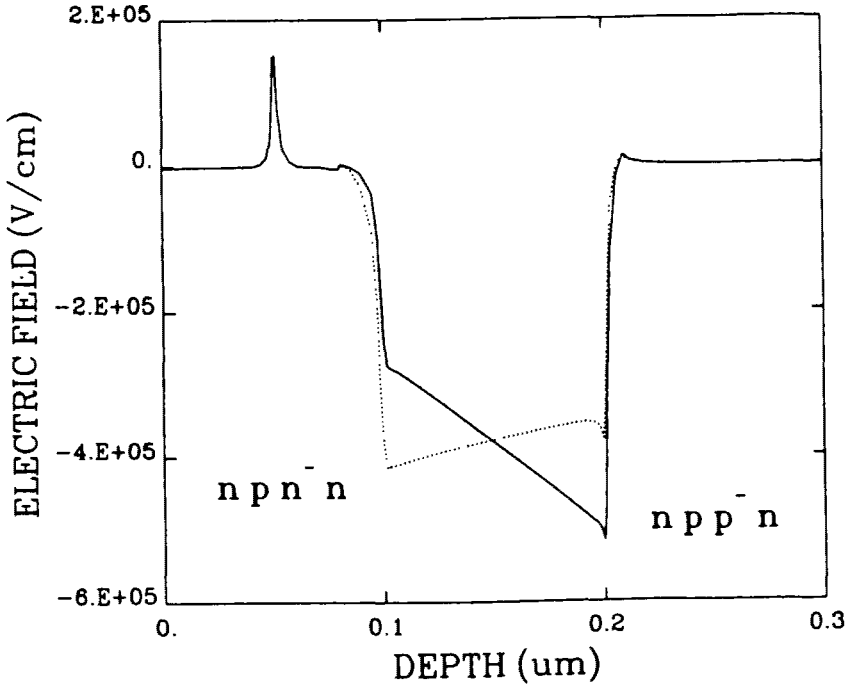

Fig. 2. Electric field profiles in the simulated devices obtained with the hydrodynamic model.

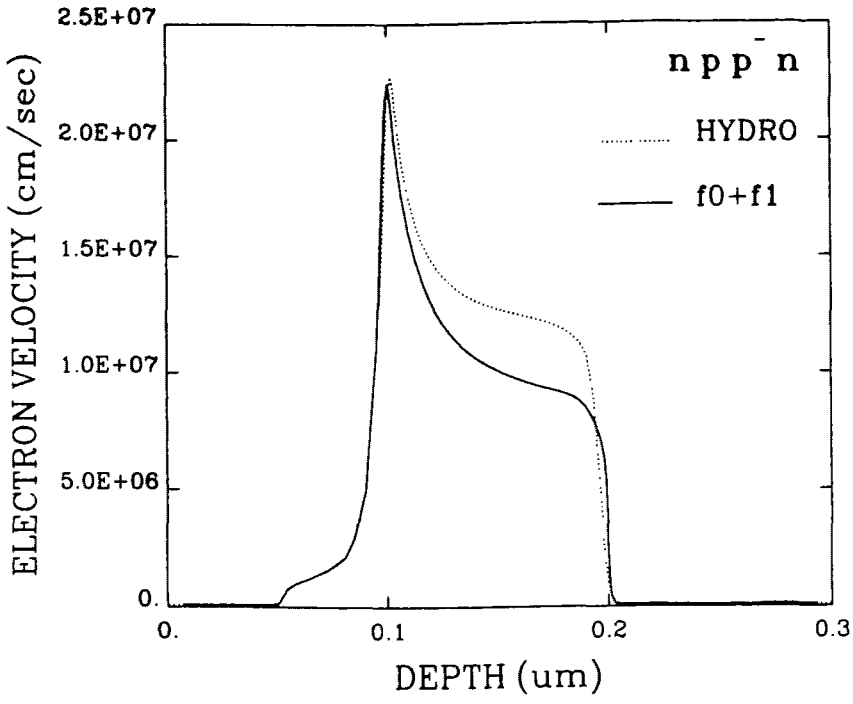

Fig. 3. Electron velocity profiles obtained with the hydrodynamic model and with the present model for the n^+-p-p^--n^+ device.

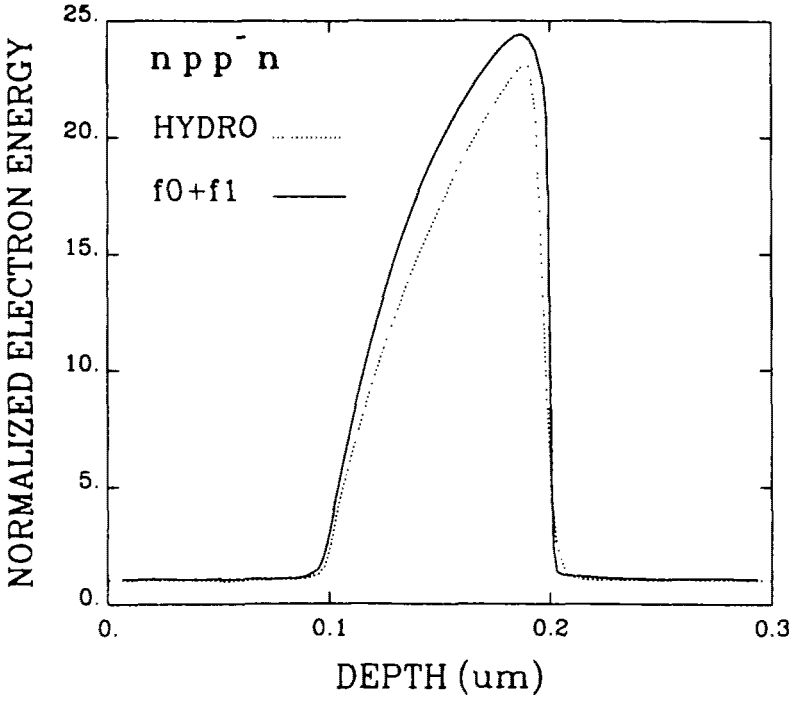

Fig. 4. Electron energy profiles normalized to the equilibrium energy $E_o = 39$ meV obtained with the hydrodynamic model and with the present model for the n^+-p-p^--n^+ device.

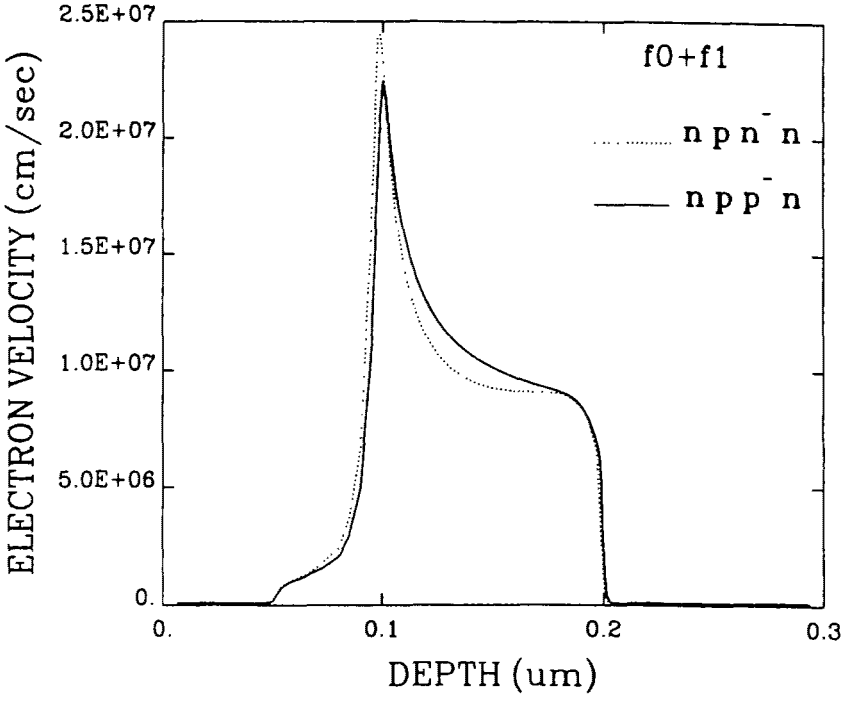

Fig. 5. Electron velocity profiles obtained with the present model for both simulated devices.

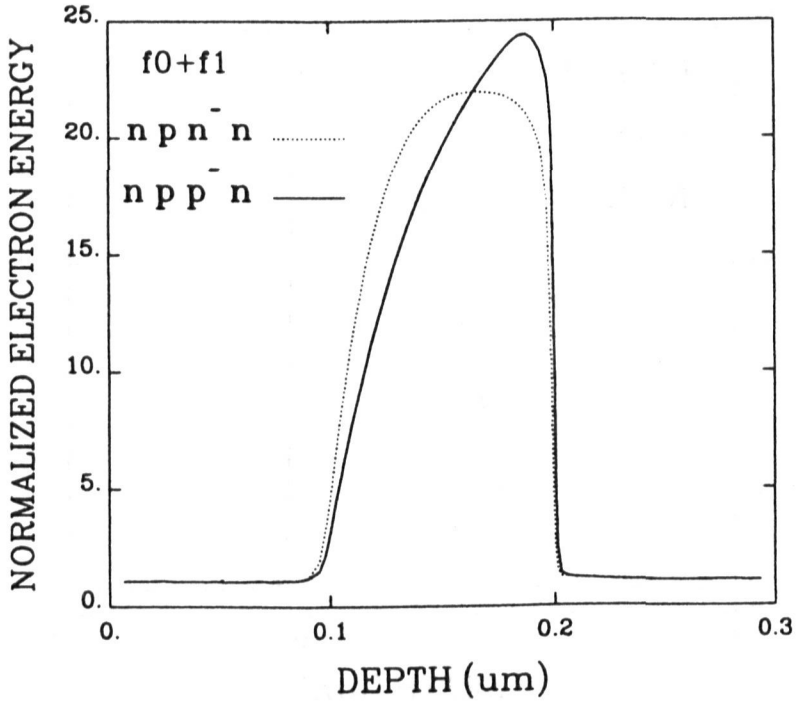

Fig. 6. Electron energy profiles normalized to the equilibrium energy $E_o = 39$ meV obtained with the present model for both simulated devices.

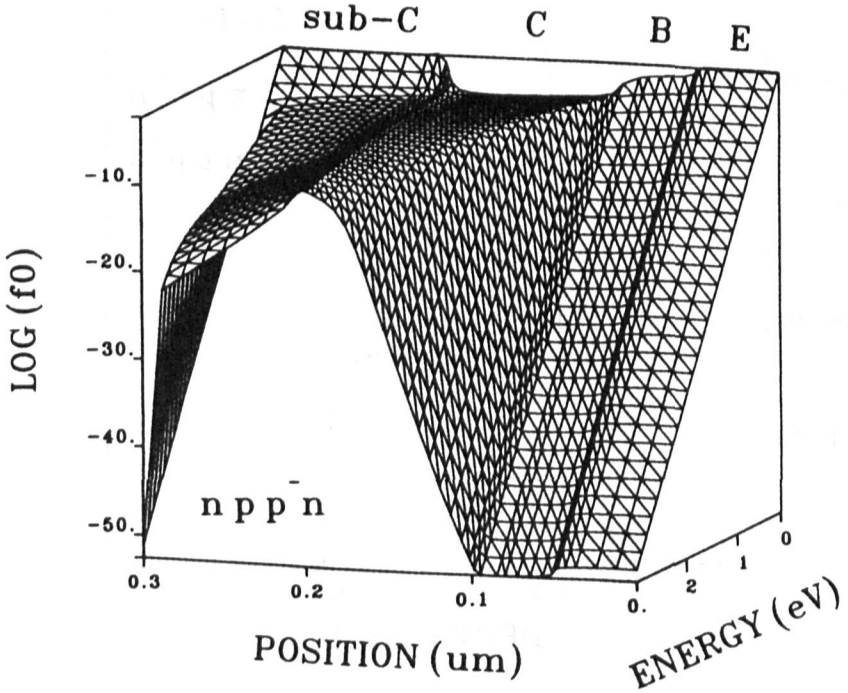

Fig. 7. Electron distribution in (E, x) space for the simulated n^+-p-p^--n^+ device.

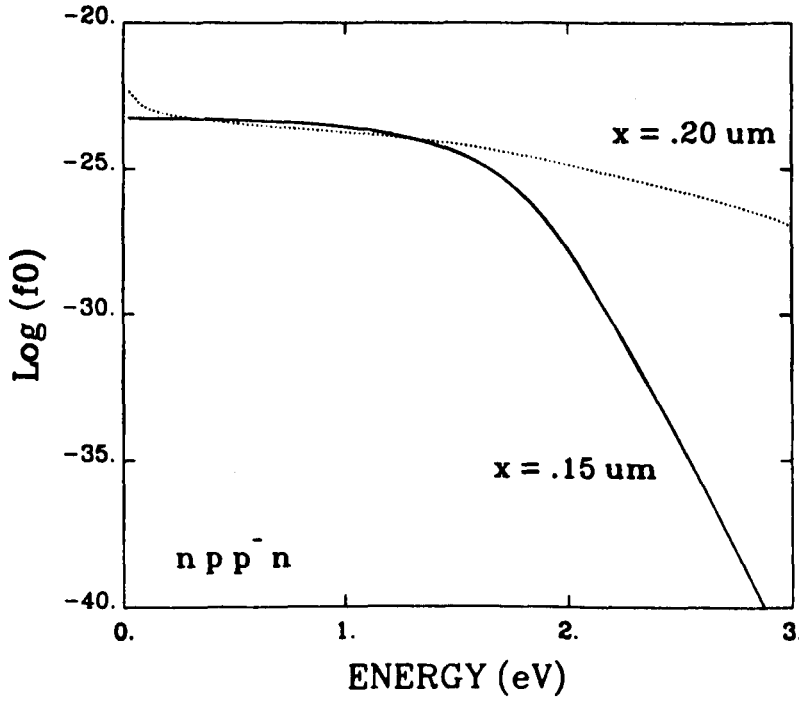

Fig. 8. Electron energy distribution for the simulated n^+-p-p^--n^+ device in two different sections with nearly the same mean energy (the normalization is such that $\int f g \mathrm{d}E = 1$).